Supporting Information

Zinc-Indium Sulfide Nanosheets with Anion Vacancies Promote Photocatalytic Upgrading of Lignin Oil to Biodiesel

Xiao Lian[†a], Jiabing Chen[†a], Jie Yang[a], Mingxiang Zhu[a], and Fang Zhang*[a]*

a. The Education Ministry Key Lab of Resource Chemistry, Shanghai Key Laboratory of Rare Earth Functional Materials, and Shanghai Frontiers Science Center of Biomimetic Catalysis, Shanghai Normal University, Shanghai 200234, China.
E-mail: zhangfang@shnu.edu.cn, mingxiangzhu@shnu.edu.cn
†These authors contributed equally.

This PDF file includes:

Supplementary Text

Figs. S1 to S48

Tables S1 to S9

Table of Contents

1.Experimental Section....3

1.1 Materials and Reagents....3

1.2 Characterization....3

2.Preparation Details....4

2.1 Preparation of $ZnIn_2S_4$....4

2.2 Substrates preparation....6

2.3 Dehydrocoupling reaction....7

2.4 Simulated real lignin oil coupling....8

2.5 Hydrodeoxygenation reaction....8

2.6 Hydrogenation of birch sawdust to lignin oil....8

3.Experimental Data....10

4. Mass Spectra....19

4.1 Substrate synthesis....19

4.2 Substrates expansion....20

4.3 GC-MS spectra of the simulated lignin-oil coupling reaction mixture....24

4.4 GC-MS spectra of styrene radical capture product....27

4.5 Main components of etherified lignin oil derived from pyrolysis of birch sawdust....27

4.6 GC-MS spectra of dimer product....28

5.References....29

1. Experimental Section

1.1 Materials and Reagents

All commercial chemicals were analytical reagents and were used without any further purification. Zn $(CH_3COO)_2 \cdot 2H_2O$, p-Cresol, CH_4N_2S, $ZnCl_2$, $InCl_3$, In $(NO_3)_3$, Cs_2CO_3, $C_3H_8O_3$, $C_2H_6O_2$ and TEMPO were purchased from Aladdin Chemistry Co., Ltd.

1.2 Characterization

The crystal structure of the sample was analyzed by powder X-ray diffraction (XRD, Rigaku Corporation, Japan) using Cu Kα radiation (λ = 0.15418 nm). The scanning electron microscope (SEM) images were captured in the S-4800 emission electron microscope manufactured by Hitachi, Ltd. of Japan. Morphologic features of the samples were examined using a JEOL-2100 transmission electron microscope manufactured by JEOL Ltd., Japan, which operates at a working voltage of 200 kV. UV-Vis diffuse reflectance spectra of all solid samples were recorded using a UV-Vis spectrophotometer (UV-Vis DRS, Shimadzu UV-2450, Japan) within the wavelength range of 200 nm to 800 nm. The specific surface area was analyzed using the BET nitrogen adsorption-desorption isotherm method with the TriStar II model from McMurray Tech, USA. X-ray photoelectron spectroscopy (XPS) and valence band XPS (VB-XPS) measurements were performed using the Thermo SCIENTIFIC K-Alpha spectrometer (Al Kα, 1486.68 eV, as the emission source). The inductively coupled plasma optical emission spectroscopy (ICP) testing was conducted using the VISTA-MPXICP-OES instrument manufactured by Varian, Inc. of the United States. The substances were analyzed using a Bruker AV 400 M model nuclear magnetic resonance spectrometer. Determining the Charge Properties of Photocatalysts Using the Zeta Sizer Ultra Nanoparticle Size Analyzer. Steady-state photoluminescence (PL) spectra were measured using the HORIBA JOBIN YVON (USA) spectrometer with optical excitation at 470 nm. The instantaneous time-current response curve (I-t), Mott-Schottky plot, and electrochemical impedance spectroscopy (EIS) were

measured using the Shanghai Chenhua CHI760E electrochemical workstation. Select the Agilent 8860 series GC to precisely calculate the amount of hydrogen gas generated by the reaction.

2. Preparation Details

2.1 Preparation of $ZnIn_2S_4$

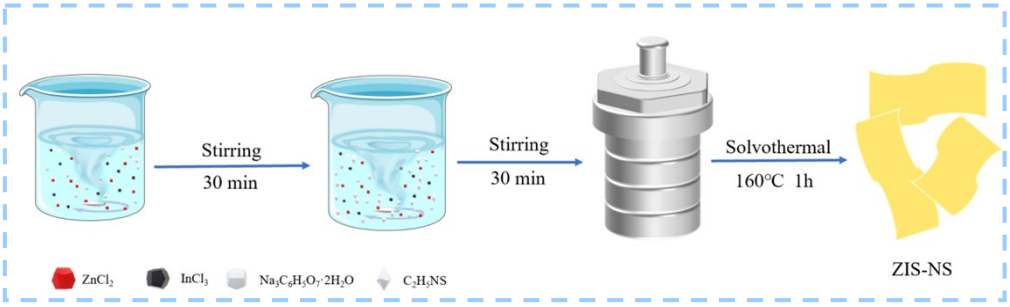

Figure S1. Synthesis flow chart of $ZnIn_2S_4$ material.

a. Preparation of ZIS-NB

ZIS-NB was prepared by a hydrothermal method. $ZnSO_4·7H_2O$ (0.25 mmol), $InCl_3·4H_2O$ (0.50 mmol), and TAA (1.00 mmol) were added into a 25 mL Teflon-lined autoclave which was filled with 12 mL pyridine as solvent. After stirring for 30 min, the mixture was transferred into a 100 mL Teflon-lined autoclave, sealed, and heated at 140 °C for 16 h. After the autoclave was naturally cooled to room temperature, the product was washed three times with absolute ethanol and deionized water respectively, and dried at 60 ℃ for 4 h to obtain ZIS-NB.[1]

b. Preparation of ZIS-NF

ZIS-NF was prepared by a hydrothermal method. $ZnSO_4·7H_2O$ (1 mmol) and $InCl_3·4H_2O$ (2 mmol) were dissolved in 20 mL of deionized water within a 100 mL beaker. Then, CTAB (0.26 g) was added to the solution under magnetic stirring until complete dissolution. Thioacetamide (TAA, 4 mmol) was added under continuous stirring. Then the mixture was transferred to a 50 mL stainless Teflon-lined autoclave, tightly sealed, and heated at 160 °C for 16 h. After the autoclave was naturally cooled to room temperature, the product was washed three times with absolute ethanol and deionized water respectively, and dried at 60 ℃ for 4 h to obtain ZIS-NF.[1]

c. Preparation of ZIS-B

ZIS-B was prepared by a hydrothermal method. $ZnCl_2$ (3 mmol), $InCl_3$ (6 mmol) and TAA (12 mmol) were dissolved in 500 mL of deionized water. The mixture was heated at 95 °C for 5 h with vigorous stirring. After the autoclave was naturally cooled to room temperature, the product was washed three times with deionized water respectively, and dried at 60 ℃ for 12 h to obtain ZIS-B.[2]

d. Preparation of ZIS-NS

ZIS-NS was prepared by a hydrothermal method. $ZnCl_2$(0.136 g), $InCl_3 \cdot 4H_2O$ (0.586 g) and $Na_3C_6H_5O_7 \cdot 2H_2O$ (0.6 g) were dissolved in 30 mL of deionized water. The mixture was stirred at room temperature for 30 minutes. Then, thioacetamide (4 mmol) was added to the above solution, followed by stirring for 30 minutes. Then the mixture was transferred to a 100 mL stainless Teflon-lined autoclave, tightly sealed, and heated at 160 °C for 1 h. After the autoclave was naturally cooled to room temperature, the product was washed three times with absolute ethanol and deionized water respectively, and dried at 60 ℃ for 12 h to obtain ZIS-NS.[3]

e. Preparation of ZIS with different sulfur vacancy concentrations

ZIS with varied sulfur-vacancy was prepared by a hydrothermal method. $ZnCl_2$ (0.136 g), $InCl_3 \cdot 4H_2O$ (0.586 g) and $Na_3C_6H_5O_7 \cdot 2H_2O$ (0.6 g) were dissolved in 30 mL of deionized water. The mixture was stirred at room temperature for 30 minutes. Then, a certain amount of thioacetamide (4.0 mmol、5.0 mmol、6.0 mmol、7.0 mmol、 8.0 mmol、9.0 mmol、10.0 mmol) was added to the above solution, followed by stirring for 30 minutes. Then the mixture was transferred to a 100 mL stainless Teflon-lined autoclave, tightly sealed, and heated at 160 °C for 1h. After the autoclave was naturally cooled to room temperature, the product was washed three times with absolute ethanol and deionized water respectively, and dried at 60 ℃ for 12 h.

2.2 Substrates preparation

a. Preparation of some substrates by etherification method

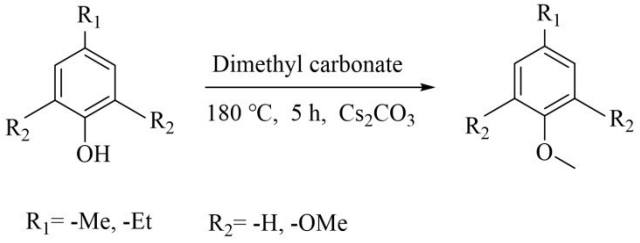

Figure S2. Preparation of some substrates by etherification method.

4-ethyl-1,2-dimethoxybenzene and 1,2-dimethoxy-4-propylbenzene were prepared by an etherification method.

Briefly, 500 mg of 4-ethyl-1,2-benzenediol, and 4-propyl-1,2-benzenediol was dissolved in 5 mL of dimethyl carbonate with 50 mg of Cs_2CO_3 in a pressure bottle and heated at 180 ºC for 5 h using an oil bath. The pressure bottle was then naturally cooled to room temperature. After etherification reaction, the mixture was filtered to remove the solid catalyst and the solvent was removed via reduced pressure distillation.

b. Reduction of ketones to prepare substrates

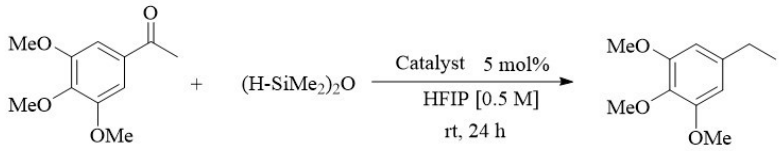

Figure S3. Reduction of ketones to prepare substrates.

The synthesis process is divided into two parts: the preparation of Catalyst, and the execution and post-treatment of the reaction.

For the preparation of Catalyst, at room temperature, 2-formylphenylboronic acid (1.20 g) is dissolved in CH_2Cl_2 (32 mL) in a round-bottomed flask and stirred for 10 minutes. Then, N-Methylhydroxylamine hydrochloride (668 mg) is added to the above mixture, and the resulting mixture is stirred at room temperature for 24 hours. After the reaction is completed, the precipitate is collected by vacuum filtration, washed with CH_2Cl_2 (6×15 mL), and dried under vacuum to obtain Catalyst as a white solid (1.48 g, yield 94%).

The reaction system is prepared using 1,2,3-trimethoxy-4-acetophenone (158

mg,), Catalyst (7.5 mg), TMDSO (292 μL), and HFIP as the solvent. The reactants are stirred at room temperature for 24 hours, then concentrated by rotary evaporation. The concentrate is purified by column chromatography (cyclohexane: ethyl acetate = 6:1) to obtain the reduced product as a clear oil, which is identified as 1,2,3-trimethoxy-4-ethylbenzene through gas chromatography-mass spectrometry (GC-MS).

c. H_2 reduction of the acrylic method for preparing some substrates

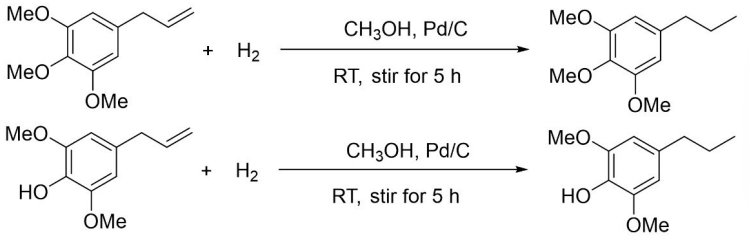

Figure S4. H_2 reduction of the acrylic method for preparing some substrates.

2.3 Dehydrocoupling reaction

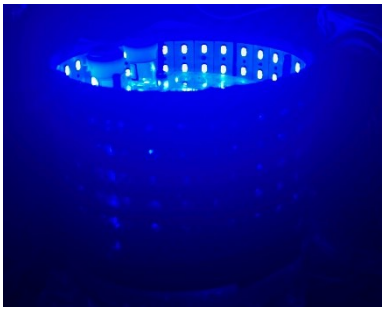

Figure S5. Photocatalytic reaction process**.**

The catalytic activity of the ZIS photocatalyst was evaluated using the self-coupling reaction of 4-methylethylbenzene as a probe reaction. Typically, 0.2 mmol of the substrate and 20 mg of catalyst were added into 3.0 mL of solvent in the quartz tube reactor, then the system was completely replaced with Ar. The reaction mixture was stirred at 1000 rpm and irradiated with an 18 W 455 nm LED light source for 12 h. After the reaction, gas-phase products (H_2) were analyzed by Agilent 8860 gas chromatograph (GC). The reaction mixture was spiked with 1,3,5-Trimethylbenzene internal standard (20 μL) and diluted with anhydrous acetonitrile (5 mL). After stirring for 10 minutes, the catalyst was filtered off, gas-phase products were

analyzed by Agilent 7890B system. Quantification of substrate conversion and dimer yield employed internal standard calibration, enabling subsequent reaction screening studies.

2.4 Simulated real lignin oil coupling

To approximate the real-world conditions of various lignin oils, we employed two sets of mixtures to simulate the photocatalytic reaction. Mixture 1 consists of 1,2,6-trimethoxy-4-propylbenzene and 1,2,6-trimethoxy-4-ethylbenzene in a molar ratio of 2:1, while mixture 2 is composed of 1,2-dimethoxy-4-propylbenzene and 1,2-dimethoxy-4-ethylbenzene, also in a 2:1 molar ratio. During the reaction, the phenolic mixtures undergo both homo-coupling and cross-coupling reactions simultaneously, generating a variety of dimers.

2.5 Hydrodeoxygenation reaction.

Hydrodeoxygenation (HDO) reactions were conducted in a 50 mL Parr autoclave with PTFE liner. The reaction mixture containing a certain mass of dimer, 20 mg catalyst, and 6 mL solvent (cyclohexane or n-hexane) was pressurized under 3 MPa H_2 after three purge cycles. Reactions proceeded at 300°C for 16 h with magnetic stirring (800 rpm).

2.6 Hydrogenation of birch sawdust to lignin oil.

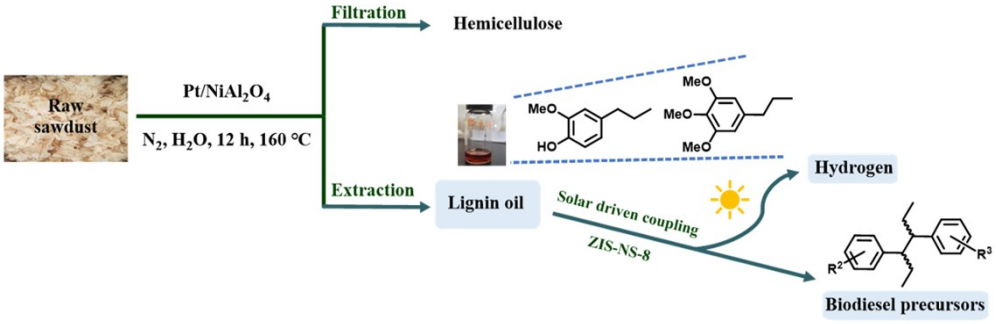

Figure S6. The process of hydrogenation of birch wood sawdust to produce lignin oil.

a. Preparation of catalysts

$NiAl_2O_4$ spinel was synthesized by a coprecipitation method at a Ni/ Al mole ratio

of 1:2.[4] A typical procedure was as follows: 40 mmol of nickel nitrate hexahydrate and 80 mmol of aluminum nitrate nonahydrate were dissolved in 200 mL of ultrapure water under vigorous stirring at room temperature. Aqueous ammonia (25−28 wt %) was added dropwise to the above solution until the pH reached 8 to obtained precipitates. Then, the formed precipitates were filtered and washed with deionized water until the pH of the filtrate reached 7. Finally, the filter cake was dried at 100 °C for 24 h followed by calcination at 800 °C for 8 h under Ar atmosphere. $Pt/NiAl_2O_4$ was prepared by the incipient wetness impregnation method with appropriate amounts of aqueous solution of chloroplatinic acid (H_2PtCl_6). The obtained samples were dried at 100 °C for 12 h and then reduced in a 10% H_2/Ar flow at 300 °C for 3 h. The Pt loading in the catalyst was 2 wt %.

b. Lignin oil monomers are prepared from wood chips

0.5 g of birch sawdust (2-5 mm) ,0.1 g of 2 wt % $Pt/NiAl_2O_4$ catalyst and 10 mL deionized water were added into the stainless steel autoclave with an internal Teflon insert. The reactor was sealed and purged with N_2 at room temperature. The reactor was heated to 160 °C for 12 h under magnetic stirring. After cooling to ambient temperature, the soluble fraction was separated from residues by centrifugation. The aqueous phase could be extracted with EA to enrich lignin monomers.

c. Etherification of lignin oils

The concentrate was dissolved in dimethyl carbonate (15 mL) and charged into a 50 mL stainless-steel autoclave. Following addition of Cs_2CO_3 (150 mg), the sealed reactor was maintained at 180°C for 5 h. After the reaction, the mixture was cooled to room temperature. The solid catalyst was removed from the reaction mixture by filtration. Dimethyl carbonate was then evaporated under reduced pressure. Subsequently, PE is used for extraction to remove polymers, resulting in a relatively pure lignin oil.

3. Experimental Data

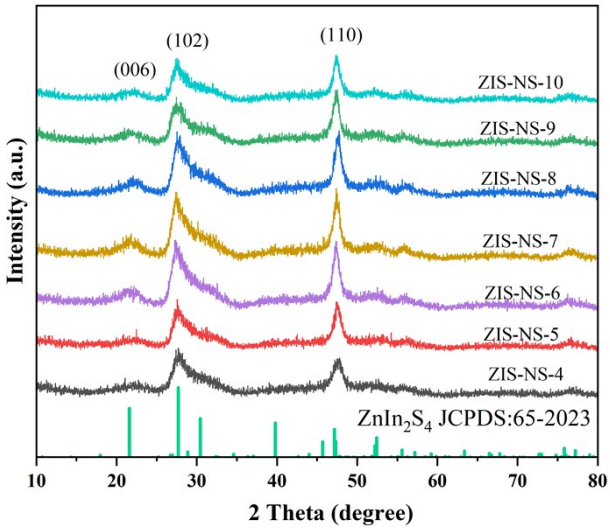

Figure S7. The XRD patterns of ZIS-NS with varied sulfur-vacancy.

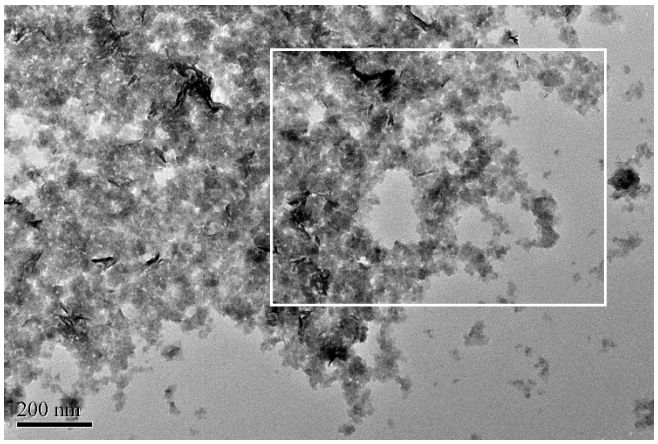

Figure S8. TEM image of $ZnIn_2S_4$ -NS-8.

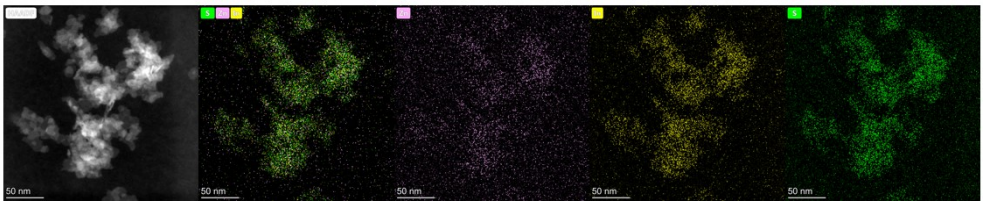

Figure S9 EDS elemental mapping images of ZIS-NS.

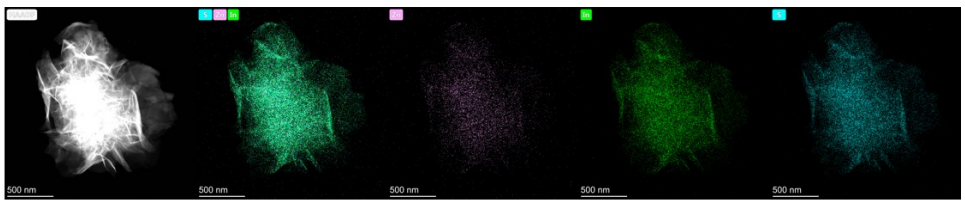

Figure S10 EDS elemental mapping images of ZIS-B.

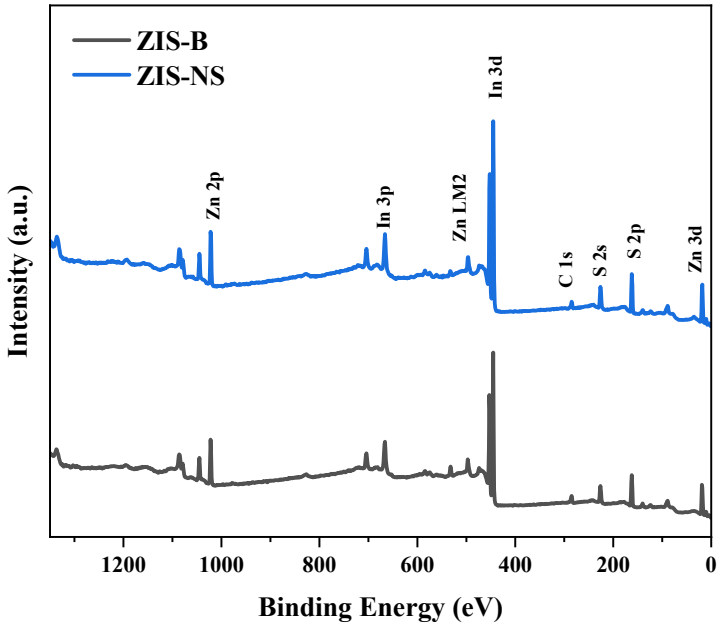

Figure S11. The XPS survey spectra of ZIS-B and ZIS-NS.

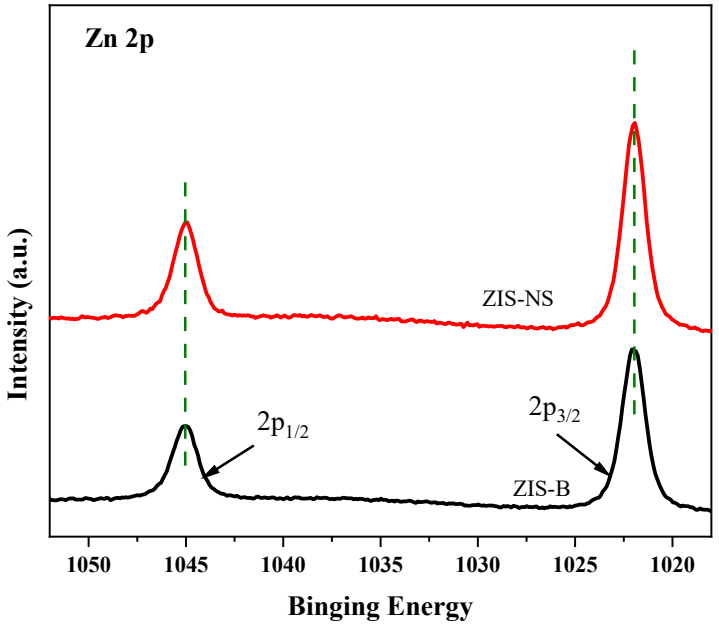

Figure S12. Zn 2p XPS spectra of ZIS-B and ZIS-NS.

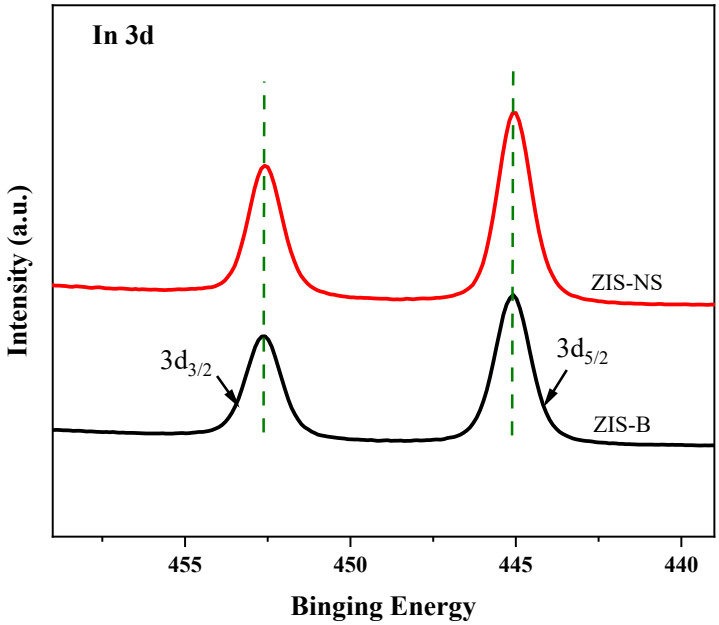

Figure S13. In 3d XPS spectra of ZIS-B and ZIS-NS.

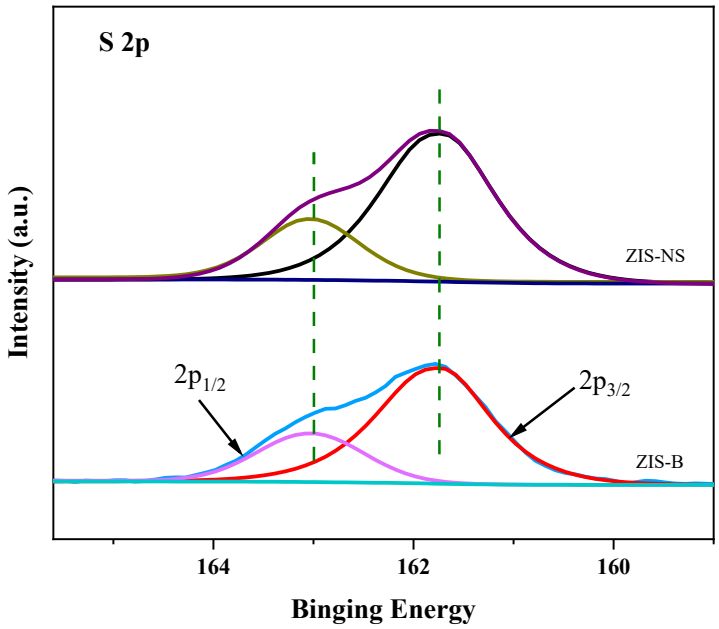

Figure S14. S 2p XPS spectra of ZIS-B and ZIS-NS.

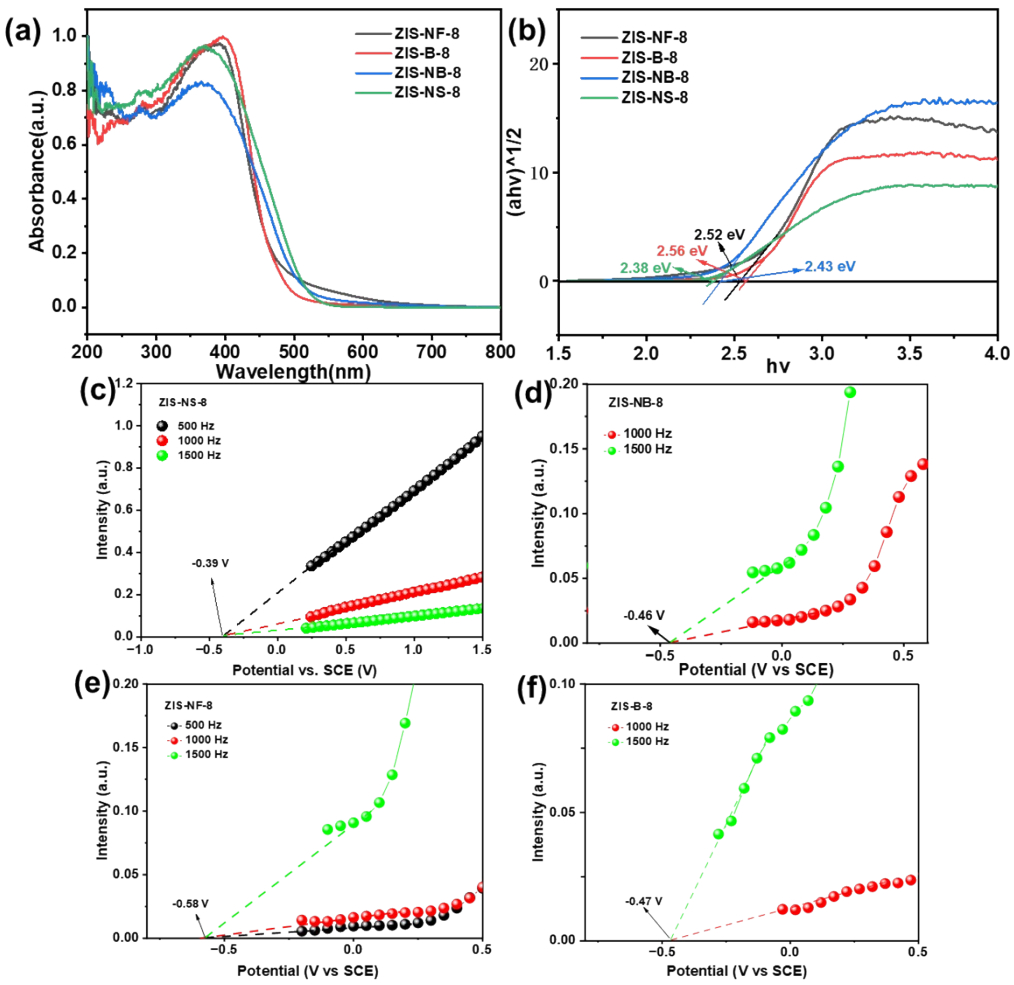

Figure S15. (a) UV-vis diffuse reflectance spectra of different morphologies of ZIS materials, and (b) the relationship between Kubelka-Munk function and photon energy; (c)-(f) Mott-Schottky.

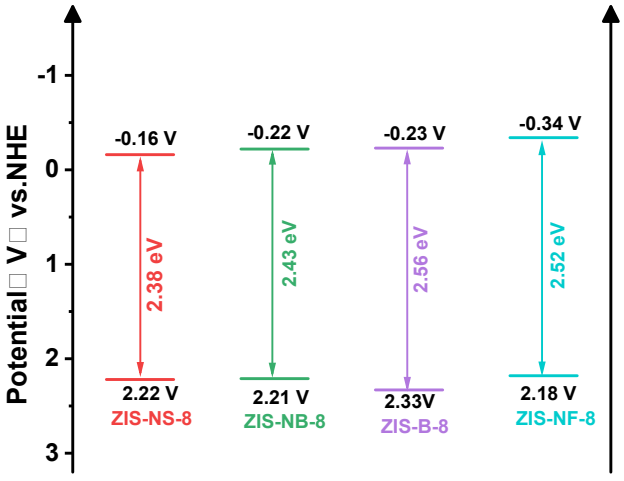

Figure S16. Band structures of ZIS with different morphology.

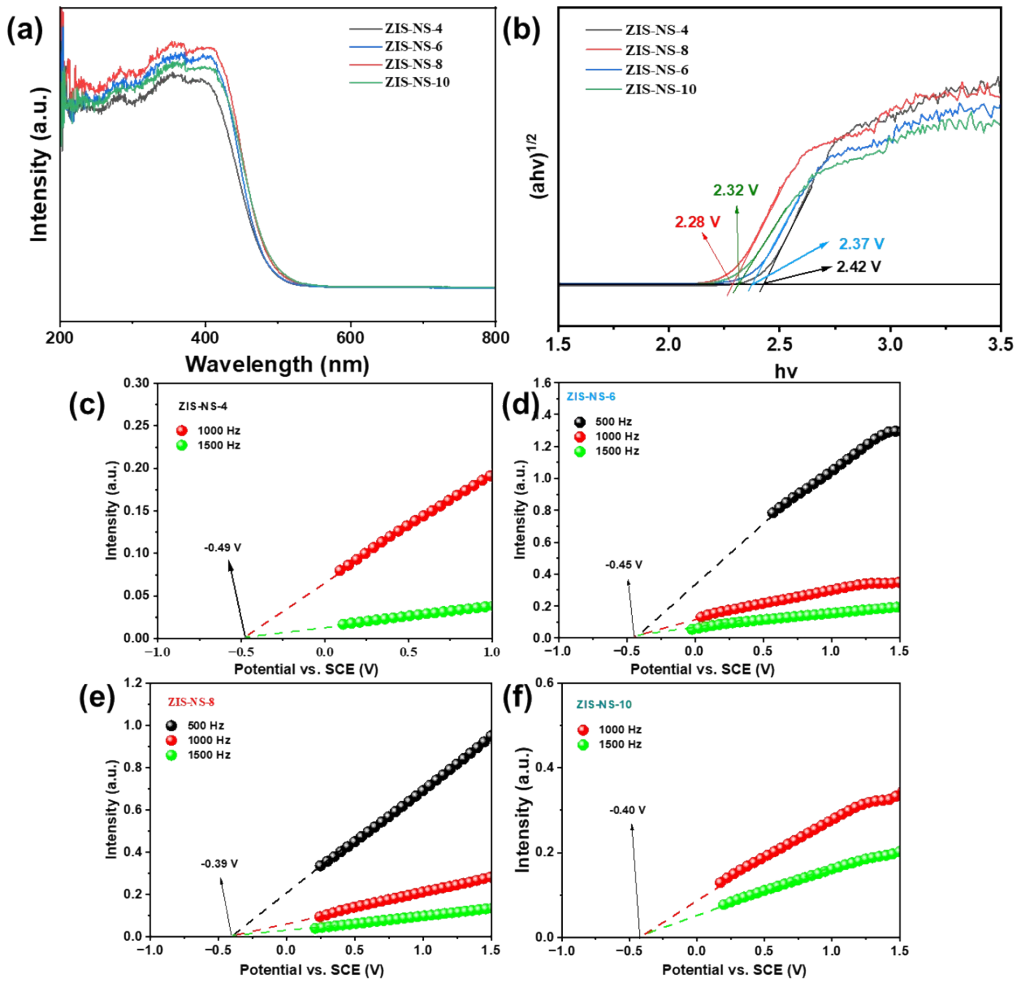

Figure S17. (a) UV-vis diffuse reflectance spectra of varied sulfur-vacancy of ZIS materials, and (b) the relationship between Kubelka-Munk function and photon energy; (c)-(f) Mott-Schottky.

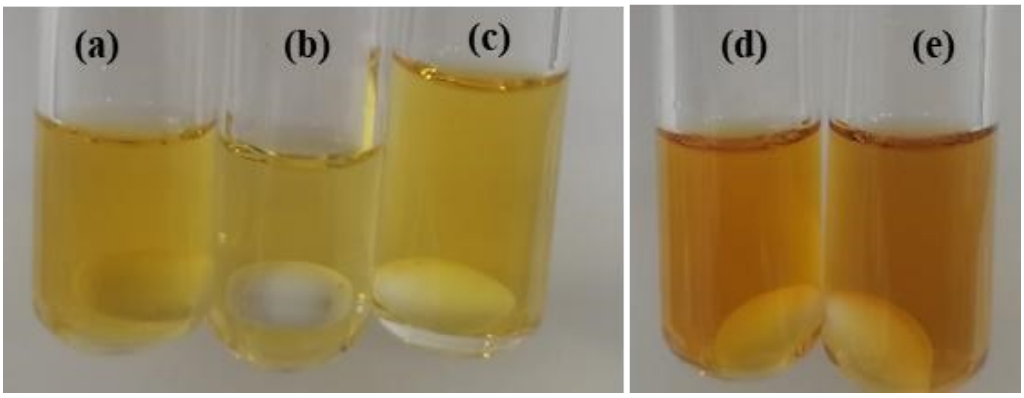

Figure S18. Etherified lignin oil (a), eucalyptus wood (b), birch wood (c), pine wood (d), corn cob (e), and metasequoia wood.

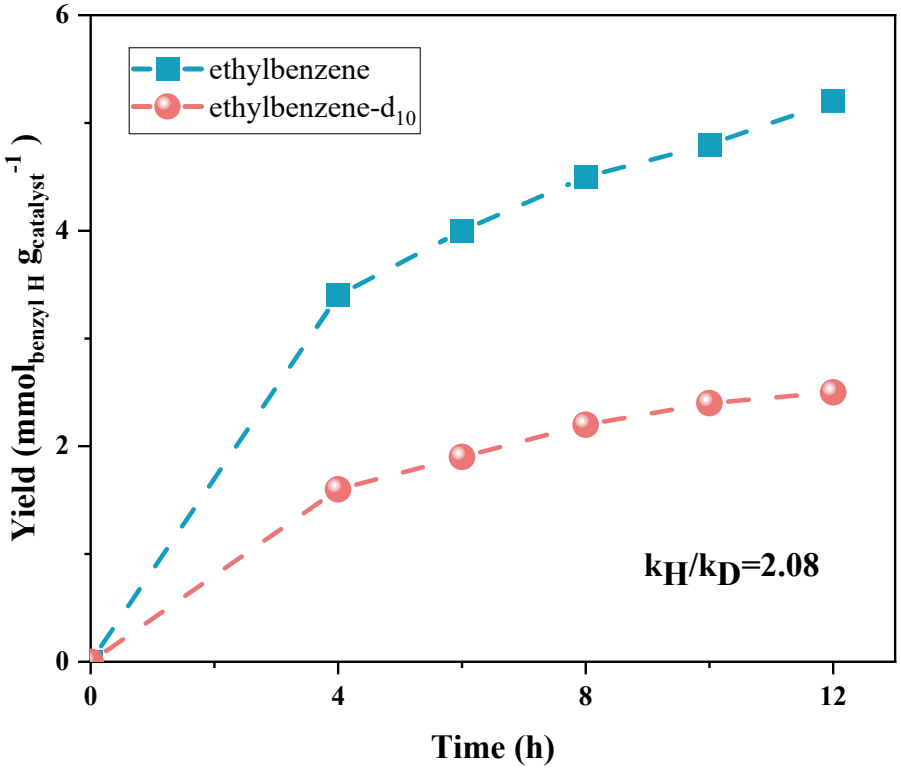

Figure S19. Kinetic isotope effect study of the photocatalytic conversion of ethylbenzene and ethylbenzene-d_{10} over ZIS-NS.

As shown in Figure S19, a kinetic isotope effect (KIE_{app}) greater than 2, measured for the coupling of ethylbenzene versus its deuterated form (d_{10}) on ZIS-NS-8, confirms that hydrogen transfer is the rate-determining step.

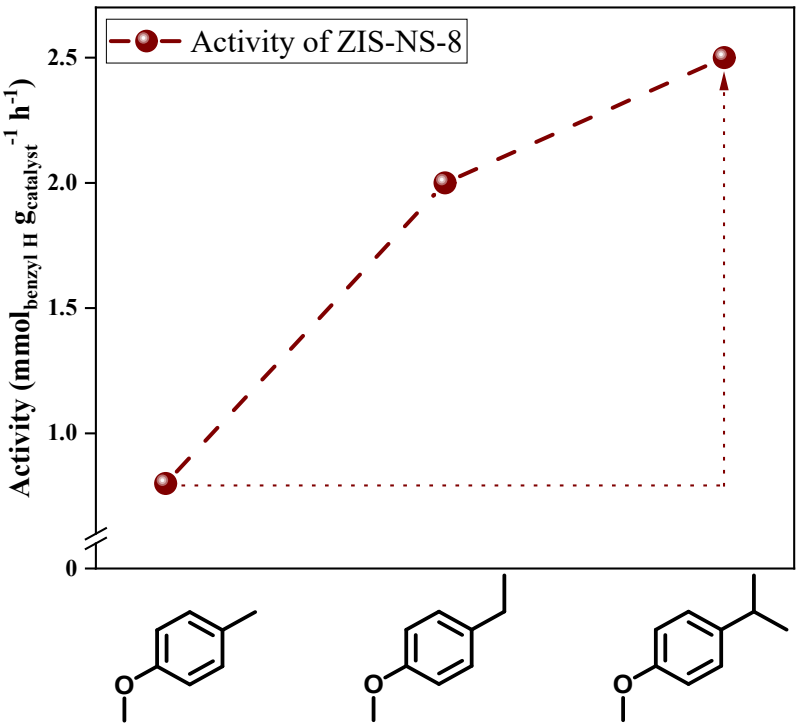

Figure S20. Dependence of C–H bond dissociation in ZIS on the coupling rate of benzyl groups.

Photocatalytic conversion experiments were conducted using several benzyl reagents with different bond dissociation energies (BDEs) (Figure S20). Subsequently, photocatalytic experiments were conducted using benzyl reagents with varying bond dissociation energies (BDEs), as shown in Figure S20. As the bond dissociation energy decreased, the activity of ZIS significantly increased, consistent with the known negative correlation between proton-coupled electron transfer (CPET) activity and bond dissociation energy.

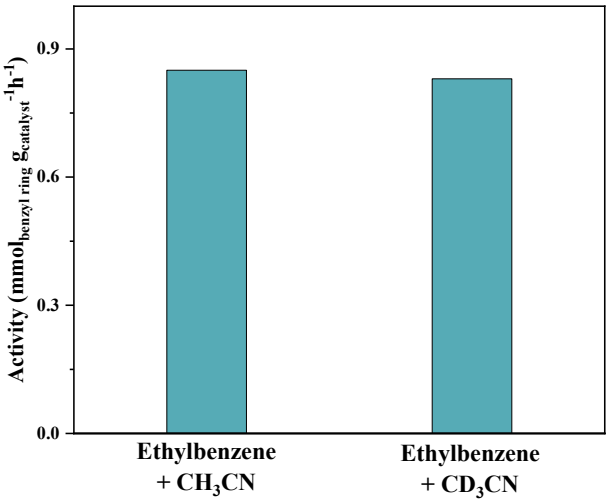

Figure S21. The coupling activity of ethylbenzene on ZIS-NS in CH_3CN and CD_3CN**.**

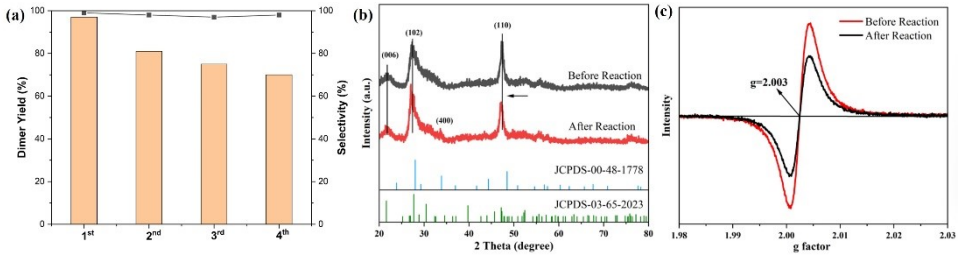

Figure S22. (a) ZIS-NS-8 cycle performance; (b) and (c) X-ray diffraction and electron spin resonance spectra before and after the ZIS-NS-8 cycle.

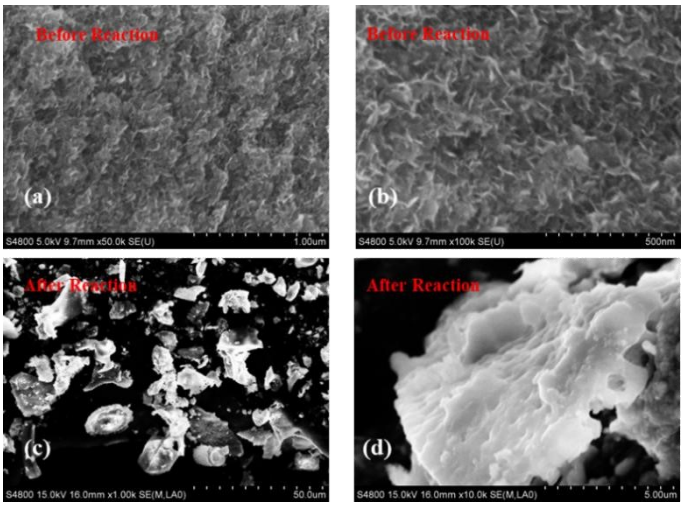

Figure S23. Scanning electron microscopy before and after the ZIS-NS-8 cycle.

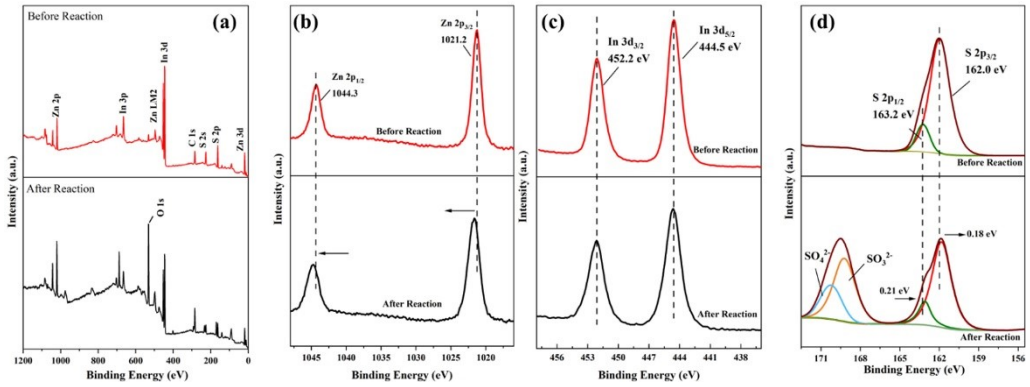

Figure S24. X-ray photoelectron spectra before and after the ZIS-NS-8 cycle.

As observed in the recycling experiments, although the product selectivity could be well maintained during repeated use, a noticeable decrease in yield was detected after the first cycle, decreasing from 97% to 81% (Fig S22a). To understand the origin of this performance decay, a comprehensive comparison of the catalyst before and after the recycling test was conducted, including analyses of crystal structure preservation, sulfur vacancy concentration, catalyst morphology, and surface elemental valence states. Based on these characterizations, the decrease in catalytic activity is reasonably attributed to the partial loss of sulfur vacancies and the deterioration of catalyst morphology, both of which are crucial to the catalytic performance in the lignin oil coupling reaction. Several possible factors may contribute to this behavior:

(1) Photocorrosion arising from relatively weak metal–sulfur bonds under prolonged photoirradiation, leading to the gradual depletion of sulfur vacancies (Fig S22c) ; (2) Structural instability of ZIS-NS-8 nanosheets, which are ultrathin in nature. Prolonged stirring during the reaction may induce nanosheet fragmentation, agglomeration, or thickening, negatively affecting catalytic accessibility and charge transfer efficiency (Fig S23) ; (3) Surface oxidation during catalyst recovery, where exposure to air during the centrifugation process may oxidize surface sulfur atoms, thereby reducing the number of active sites (Fig S24)

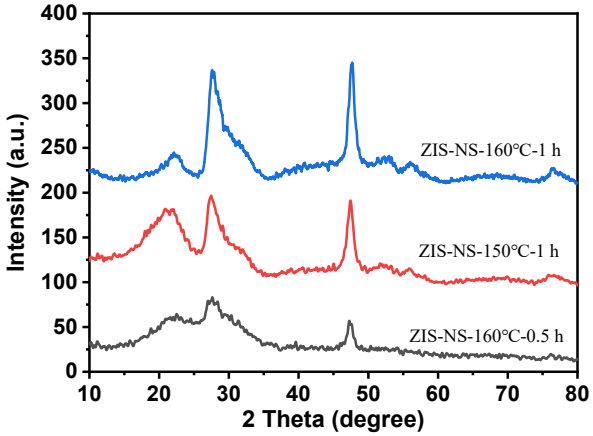

Figure S25. XRD for ZIS-NS-150 ℃ -1 h， ZIS-NS-160 °C -0.5 h and ZIS-NS-160 °C-0.5 h.

Table S1. BET surface areas of ZIS with different morphology.

Entry	Sample	BET Surface Area (m^2 /g)
1	ZIS-NB-8	19
2	ZIS-NF-8	20
3	ZIS-B-8	70
4	ZIS-NS-8	183.92

The BET specific surface area of the optimal catalyst ZIS-NS-8 with different morphologies, with the results shown in Table S1. Both catalyst morphology and surface sulfur vacancy concentration influence the reaction activity; however, the sulfur vacancy concentration plays a more dominant role in governing the catalytic performance.

Table S2. BET surface areas of ZIS-NS with varied sulfur-vacancy.

Entry	Sample	BET Surface Area (m^2/g)	Pore Volume (cm^3/g)	Pore Size (nm)
1	ZIS-NS-4	161	0.22	5.85
2	ZIS-NS-6	176	0.23	5.27
3	ZIS-NS-8	183	0.25	5.48
4	ZIS-NS-10	136	0.19	5.63

Table S3. Atomic ratio of Zn, In, and S in ZIS-NS-4 and ZIS-NS-8 (via EDS).

Entry	Sample	Zn	In	S
1	ZIS-NS-4	0.91	2	3.71
2	ZIS-NS-8	0.88	2	3.35

Table S4. Atomic ratio of Zn, In, and S in ZIS-NS-4 and ZIS-NS-8 by XPS.

Entry	Sample	Zn	In	S
1	ZIS-NS-4	0.95	2	3.91
2	ZIS-NS-8	0.96	2	3.65

Table S5. Activity of visible light catalyzed C-C coupling in different solvents.

Entry	Solvent	Conversion(%)	Dimer yield(%)	Selectivity(%)
1	CH_3CN	90	90	99
2	H_2O	43	34	69
3	DMF	12	9	75
4	DMA	28	15	53
5	DMSO	50	31	62
6	CH_2Cl_2	56	40	72
7	$CHCl_3$	17	13	75

Reaction conditions: 2.0 mmol of 4-methoxyethylbenzene, 20 mg of ZIS-NS-8, solvent (0.67 M), 455 nm LED (18W) irradiation, Ar atmosphere. Dimer yield (wt %) was determined by GC-MS, using mesitylene as the internal standard. H_2 yield (%) was quantified using the external standard

method.

Table S6. Reaction condition screening for lignin oil model compounds.

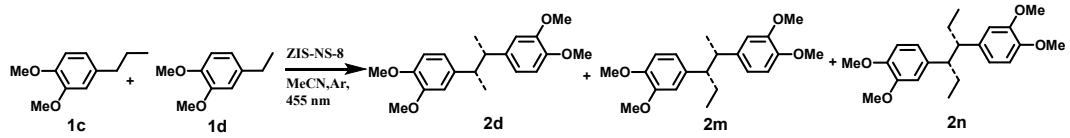

Entry	Time (h)	Yield 2d (%)	Yield 2m (%)	Yield 2n (%)
1	1	3	6	4
2	2	8	16	8
3	4	10	23	13
4	6	11	28	27
5	12	15	36	38

Reaction conditions: 0.2 mmol of substrate, 20 mg of ZIS-NS-8, CH3CN (0.67 M), 455 nm LED irradiation for 14 h, Ar atmosphere. b) Reaction conditions: mixture (1c:1d = 2:1), 20 mg of ZIS-NS-8, CH3CN (0.67 M), 455 nm LED irradiation, Ar atmosphere. Product yield was determined by GC, using mesitylene as the internal standard.

To clarify this issue, additional time-resolved control experiments were conducted to re-examine the coupling process of the simulated lignin oil system (Table S6). The updated results clearly demonstrate that the cross-coupling products indeed dominate the coupling reaction during the initial 4 hours. After 4 hours, the decrease in the concentration of substrate 1d in the reaction slows down both the cross-coupling and its self-coupling rates. Simultaneously, mixtures 1a and 1b also follow the aforementioned pattern.

Table S7. Performance test for ZIS-NS-150 ºC -1 h , ZIS-NS-160 ºC -0.5 h and ZIS-NS-160 ℃-1 h.

Catalyst	Time (h)	Yield (%)
ZIS-NS-160 ºC -0.5 h	12	82
ZIS-NS-150 ℃-1 h	12	45
ZIS-NS-160 ºC 1 h	12	93

Reaction conditions: 0.2 mmol of substrate, 20 mg of catalyst, CH_3CN (0.67 M), 455 nm LED irradiation for 12 h, Ar atmosphere.

Table S8. Performance of ZIS-NS catalysts compared with literature reports.

Catalyst	Dosage	Irraditon	Time	Solvent	Dimer yield	References
Au-CdS	5 mg	455 nm LED	24 h	CH_3CN	83	[5]
CdSe QDs/B-SiO_2	20 mg	460 nm LED	12 h	H_2O	90	[6]
$Zn_2In_2S_5$	20 mg	200 W mercury-xenon lamp	14 h	CH_3CN	76	[7]
Vs-$ZnIn_2S_4$-NS	20 mg	455 nm LED	12 h	CH_3CN	95	Our work

Comparative studies were conducted against Au–CdS, CdSe QDs/B–SiO_2, and $Zn_2In_2S_5$ (Table S8). The results demonstrate that the present catalyst achieves superior catalytic performance under conditions that avoid the use of noble metals and toxic Cd-containing components. Furthermore, compared with previously reported $Zn_2In_2S_5$ systems, the catalytic efficiency is effectively enhanced through deliberate morphology control and sulfur vacancy engineering. These results collectively reveal that both catalyst morphology and sulfur vacancy concentration play critical roles in governing the catalytic performance.

Table S9. Mass fractions of three different atoms in ZIS by ICP-OES.

Entry	Sample	Zn (wt%)	In (wt%)	S (wt%)
1	ZIS-NS-4	13.24	40.37	23.34
2	ZIS-NS-8	13.43	44.08	26.80

4. Mass Spectra

4.1 Substrate synthesis

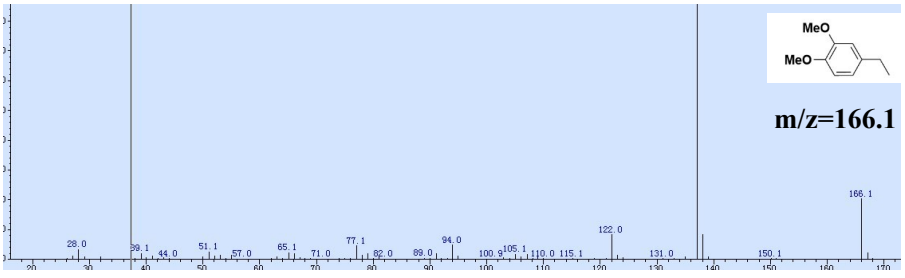

Figure S26. GC-MS spectrum of 4-Ethyl-1,2-Dimethoxybenzene.

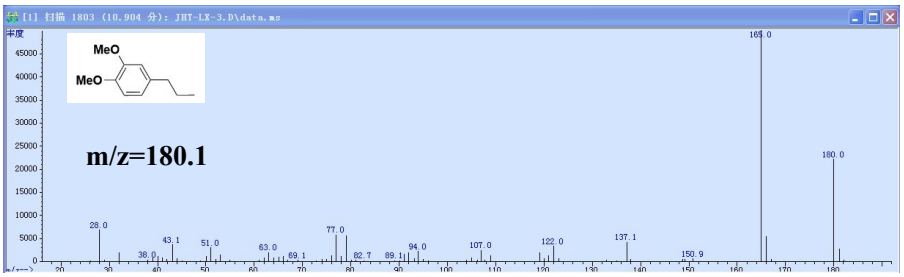

Figure S27. GC-MS spectrum of 1,2-dimethoxy-4-propylbenzene.

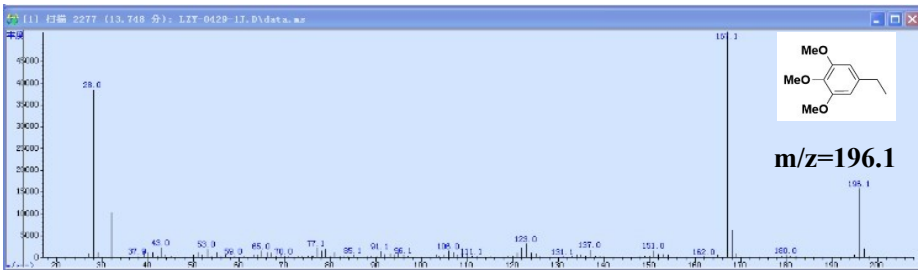

Figure S28. GC-MS spectrum of 4-ethyl-1,2,3-trimethoxybenzene.

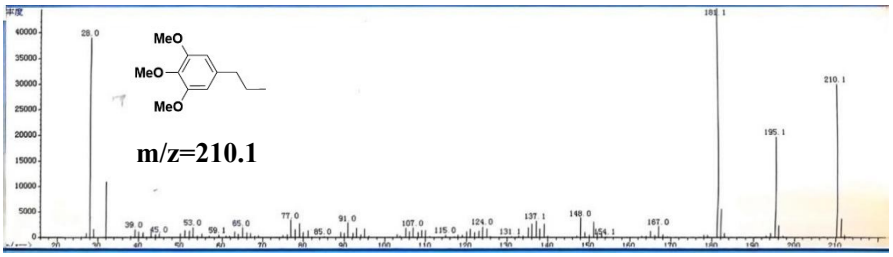

Figure S29. GC-MS spectrum of 1,2,3-trimethoxy-4-propylbenzene.

4.2 Substrates expansion

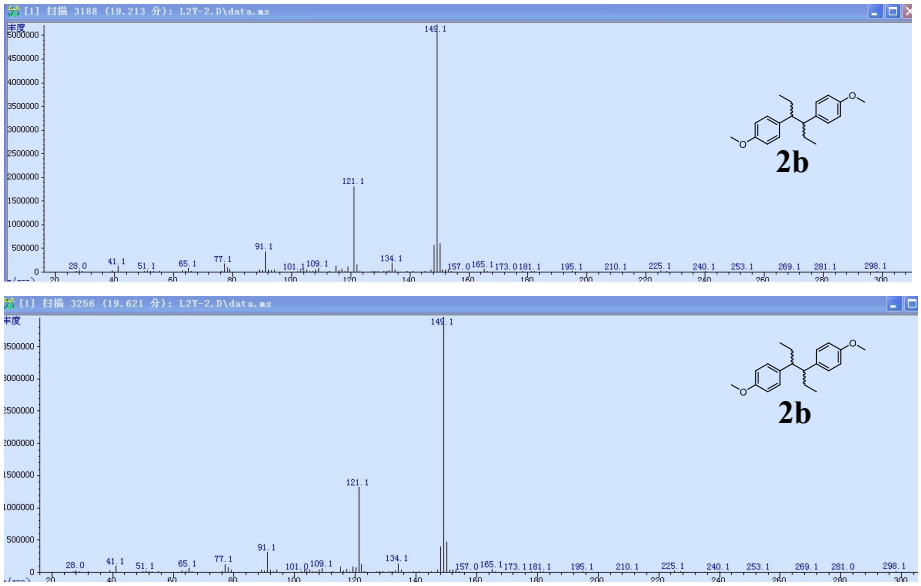

Figure S30. GC-MS spectrum of **2b**

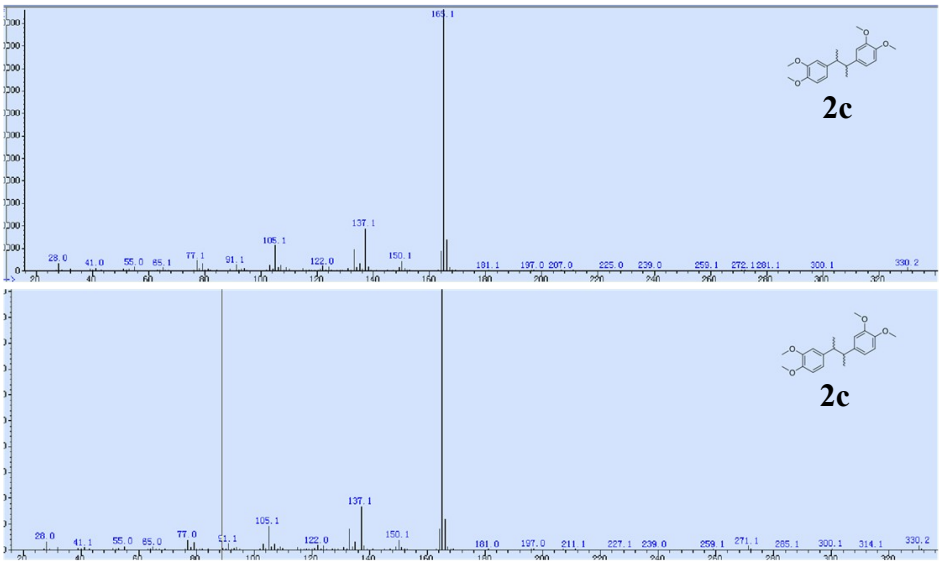

Figure S31. GC-MS spectrum of **2c**

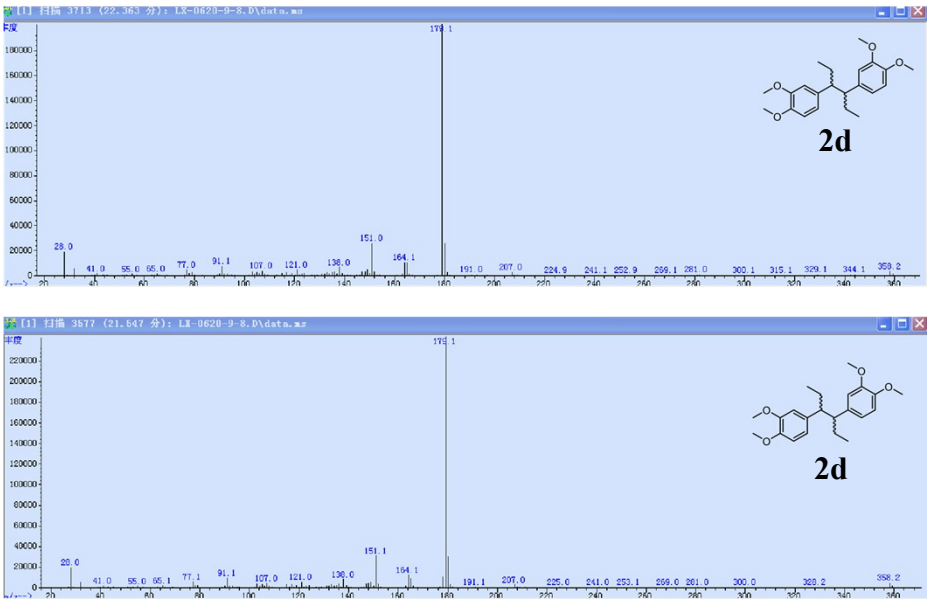

Figure S32. GC-MS spectrum of **2d**

Figure S33. GC-MS spectrum of **2e**

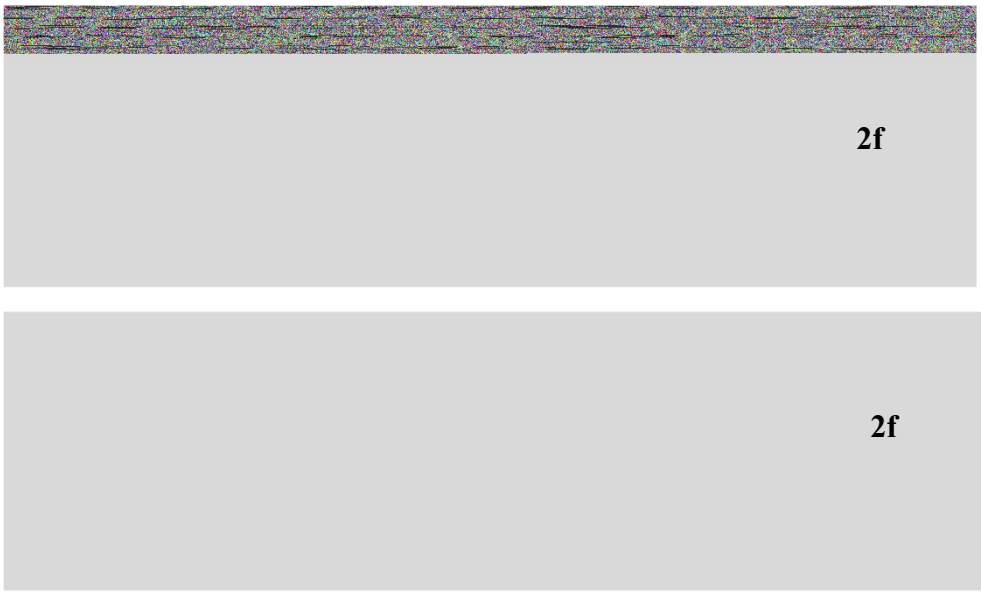

Figure S34. GC-MS spectrum of **2f**

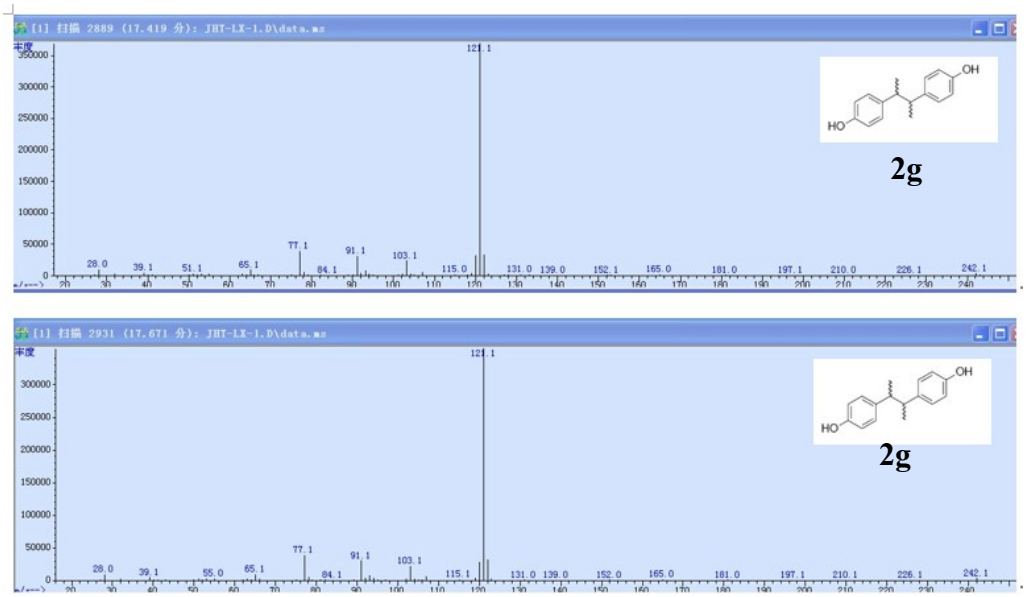

Figure S35. GC-MS spectrum of **2g**

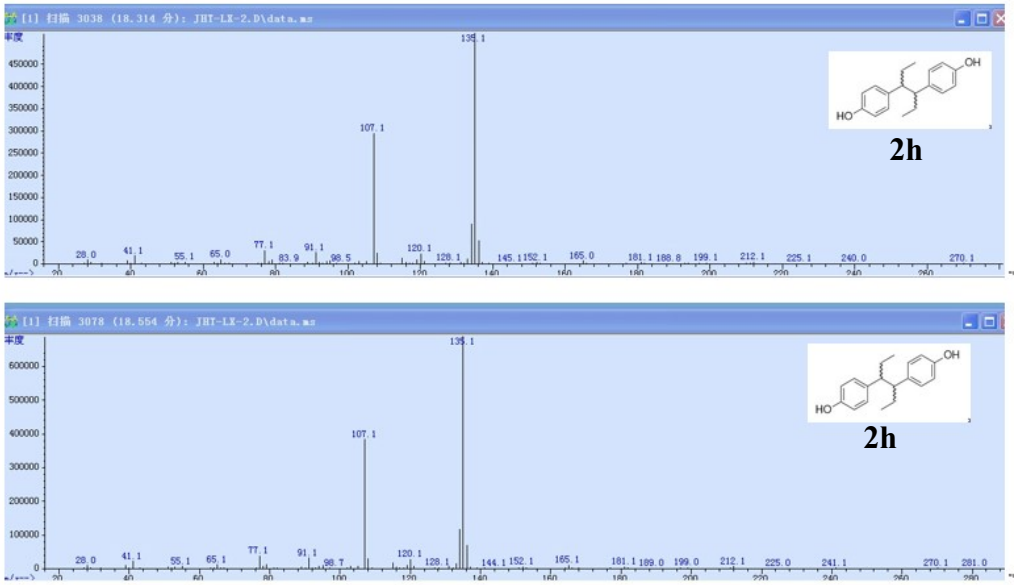

Figure S36. GC-MS spectrum of **2h**

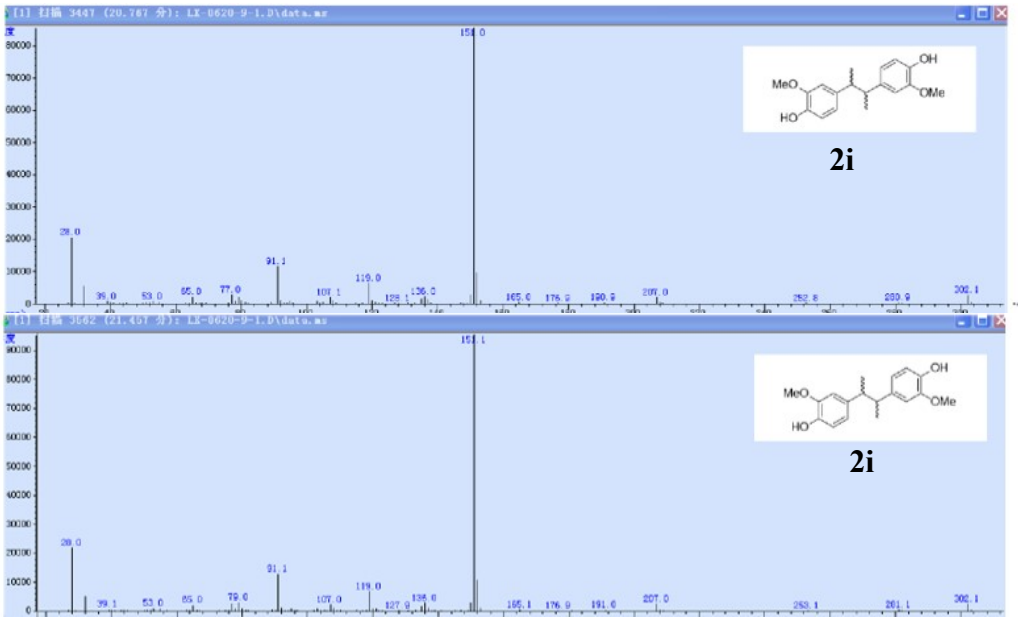

Figure S37. GC-MS spectrum of **2i**

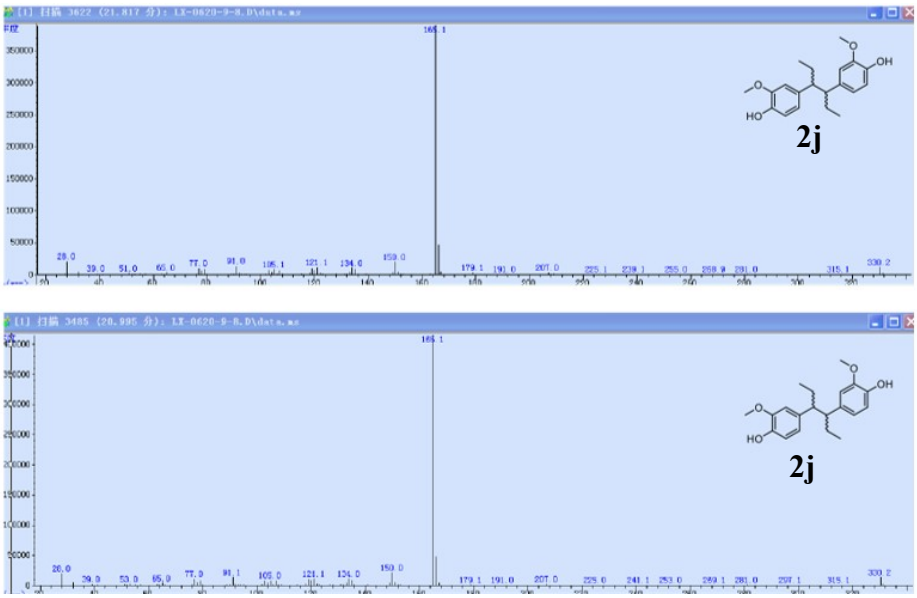

Figure S38. GC-MS spectrum of **2j**

4.3 GC-MS spectra of the simulated lignin-oil coupling reaction mixture

Compound 1

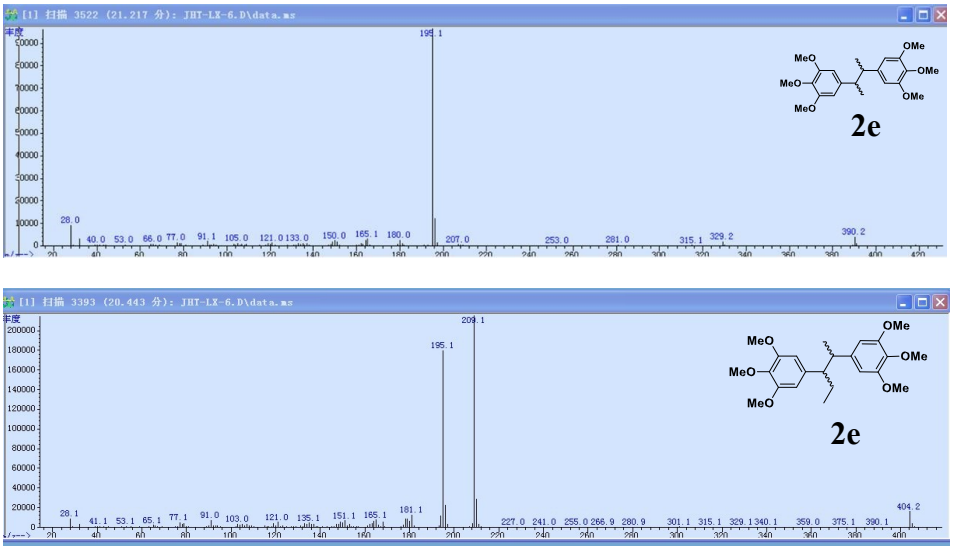

Figure S39. GC-MS spectrum of **2e**

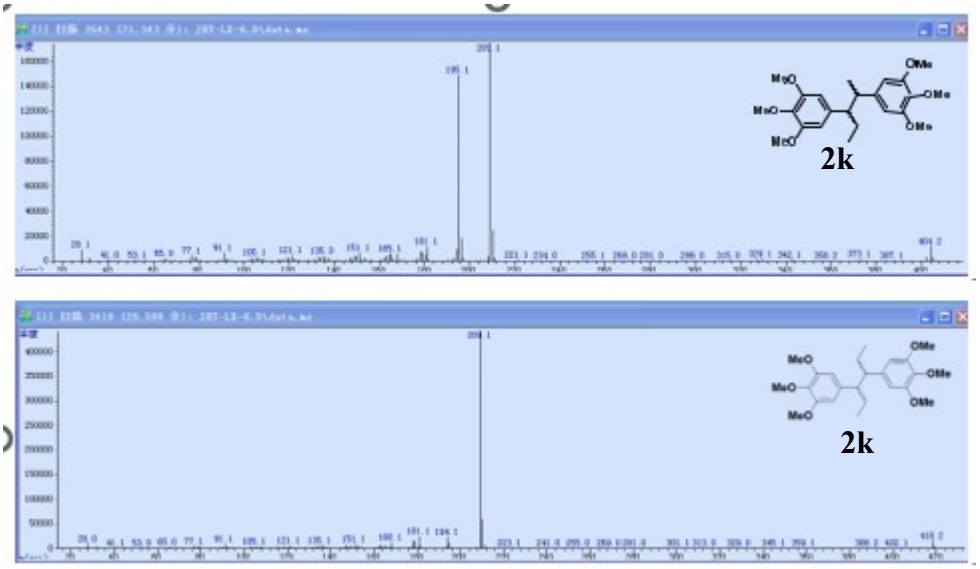

Figure S40. GC-MS spectrum of **2k**

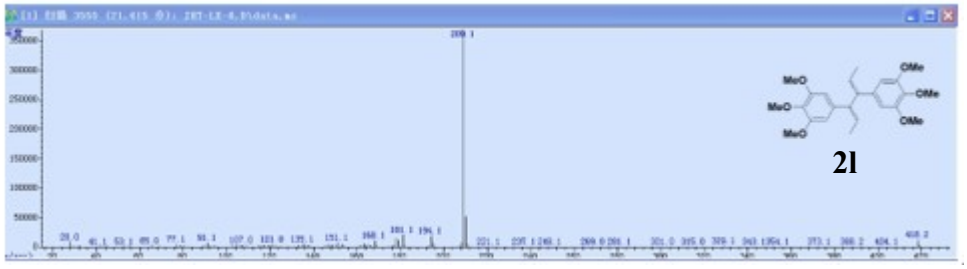

Figure S41. GC-MS spectrum of **2I**

Compound 2

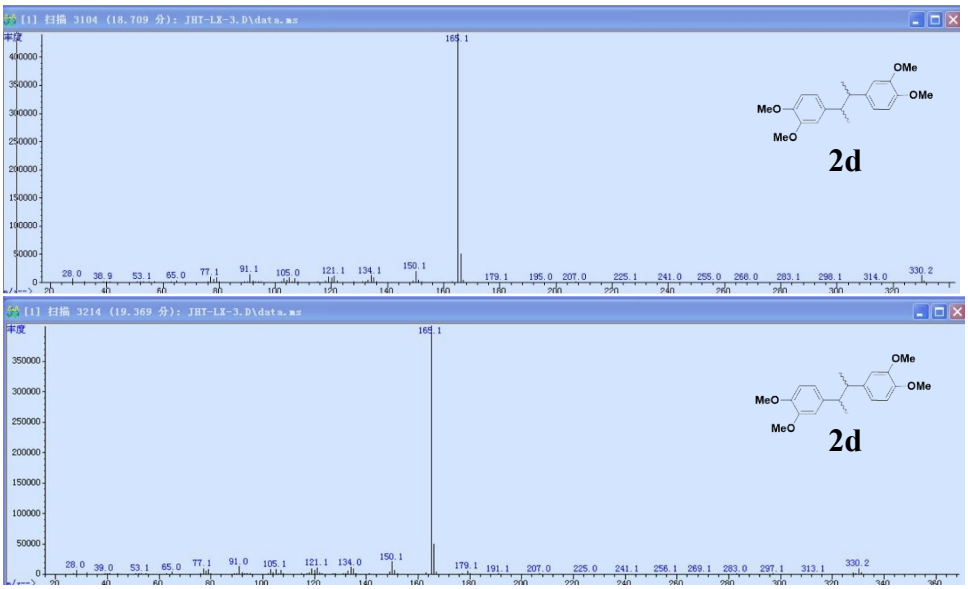

Figure S42. GC-MS spectrum of **2d**

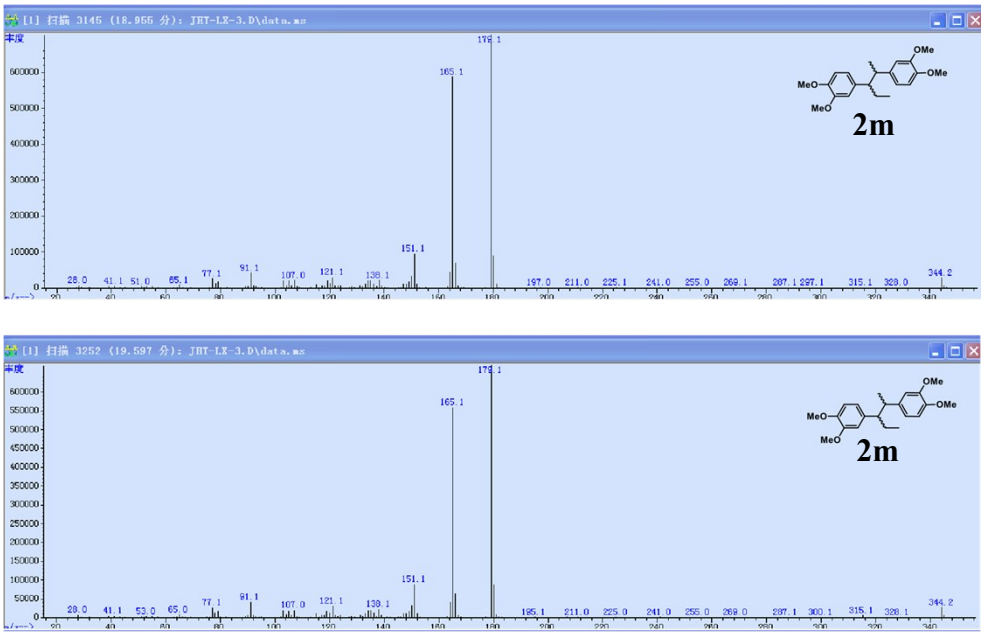

Figure S43. GC-MS spectrum of **2m**

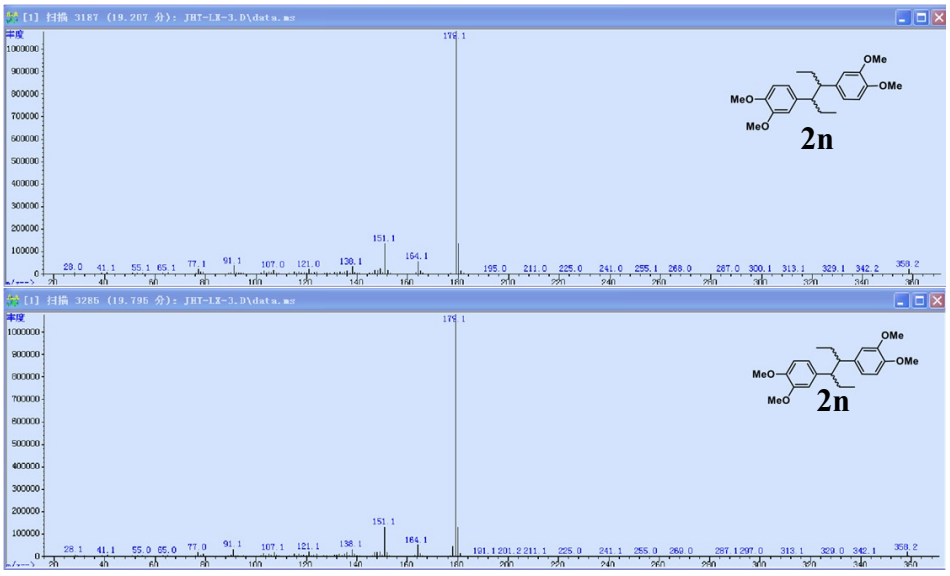

Figure S44. GC-MS spectrum of **2n**

4.4 GC-MS spectra of styrene radical capture product

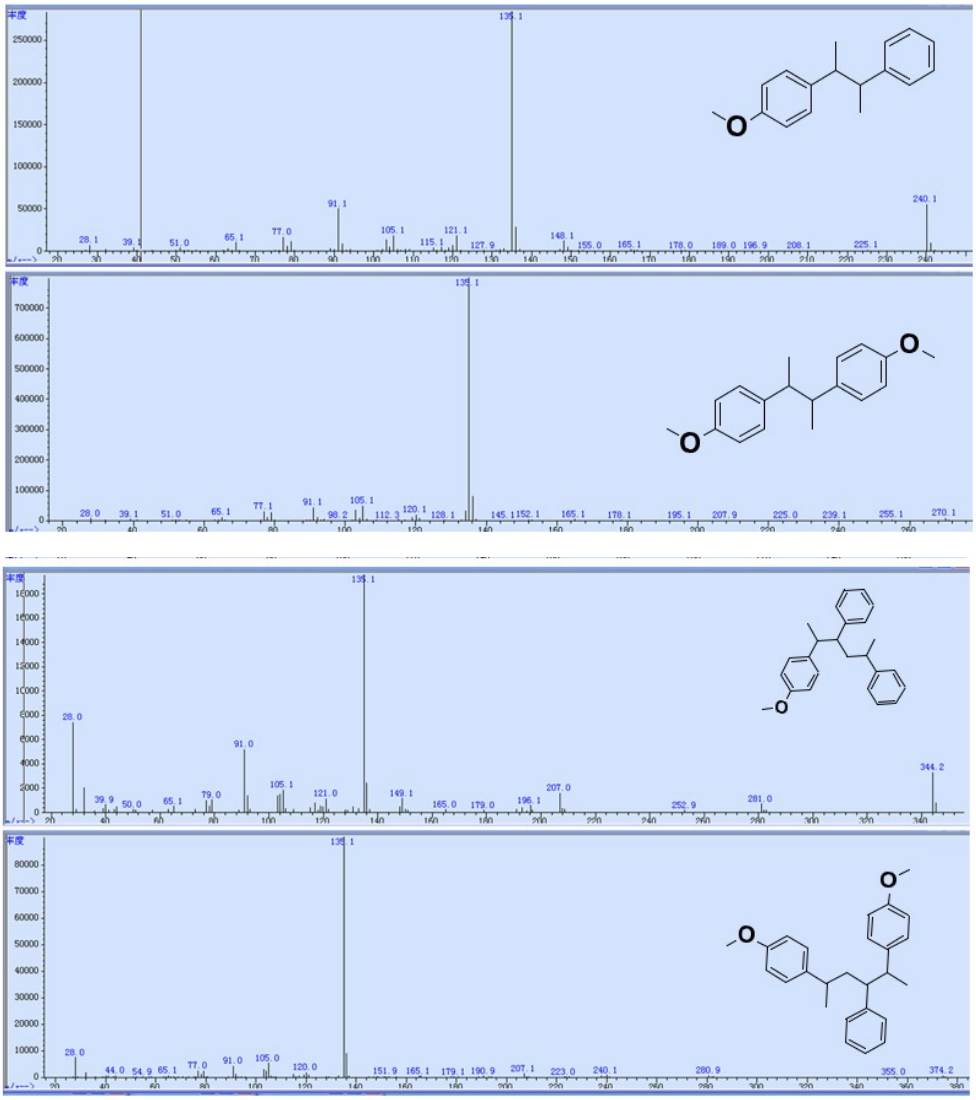

Figure S45. GC-MS spectra of styrene radical capture product

4.5 Main components of etherified lignin oil derived from pyrolysis of birch sawdust

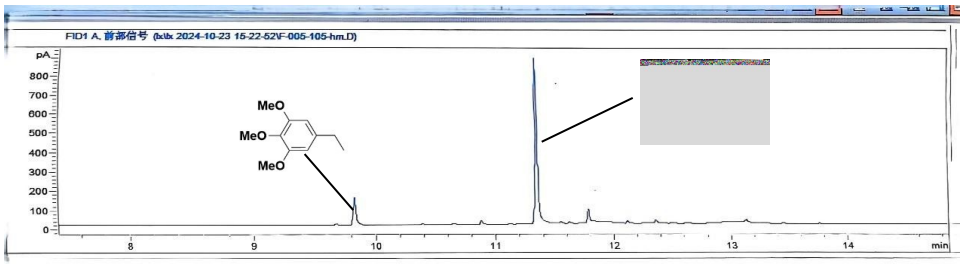

Figure S46. Lignin oil obtained from processed birch wood chips

4.6 GC and GC-MS spectra of genuine lignin (birch wood chips) coupling product

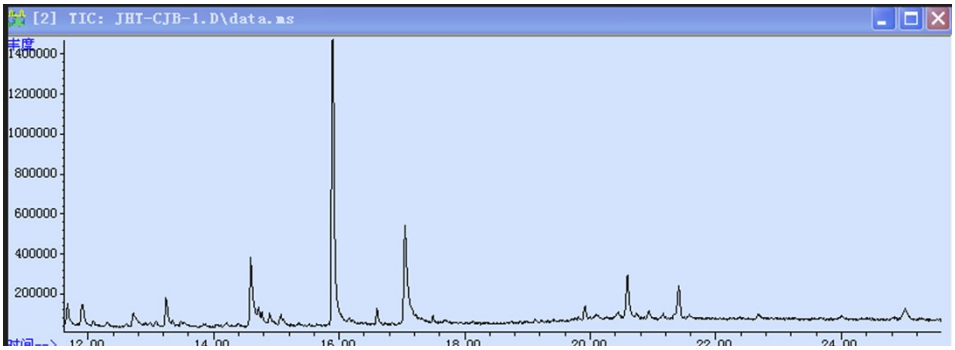

Figure S47. GC spectra of genuine lignin (birch wood chips) coupling product

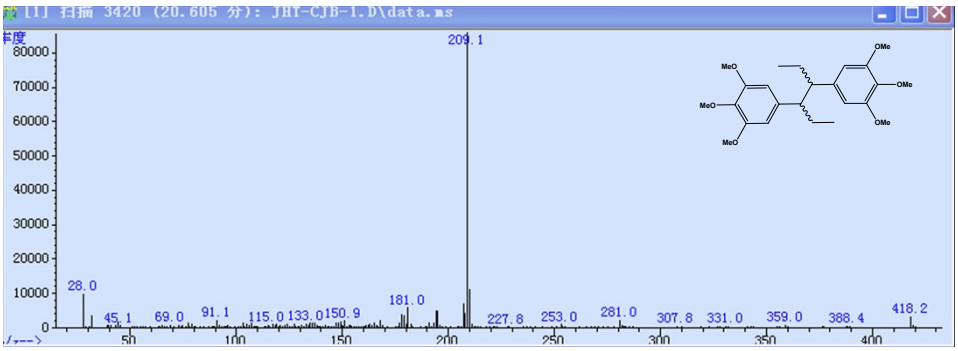

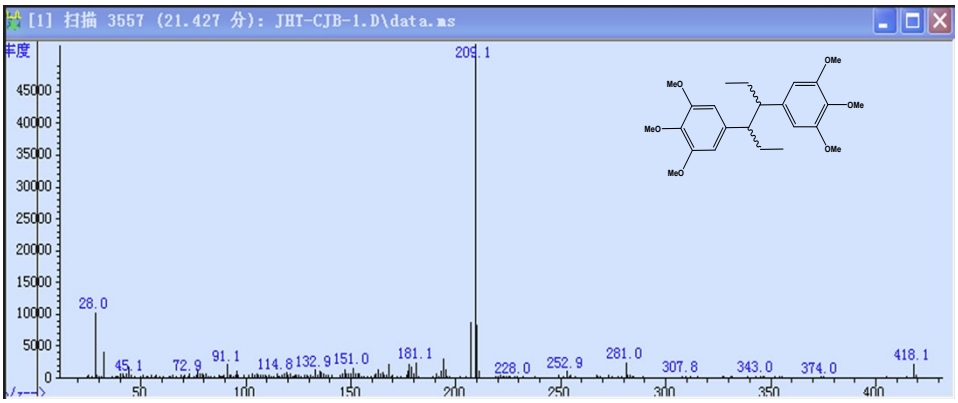

Figure S48. GC-MS spectra of genuine lignin (birch wood chips) coupling product

5. References

[1] X. Gou, *et al.*, Shape-Controlled Synthesis of Ternary Chalcogenide $ZnIn_2S_4$ and $CuIn(S,Se)_2$ Nano-/Microstructures via Facile Solution Route, *J. Am, Chem. Soc*, 2006, **128**, 7222-7229.

[2] Z. Wang, *et al.*, Exfoliated Ultrathin $ZnIn_2S_4$ Nanosheets with Abundant Zinc Vacancies for Enhanced CO_2 Electroreduction to Formate, *ChemSusChem*, 2021, **14**, 852-859.

[3] M. Tan, *et al.*, Boosting Photocatalytic Hydrogen Production via Interfacial Engineering on 2D Ultrathin Z-Scheme $ZnIn_2S_4$/g-C_3N_4 Heterojunction, *Adv. Funct. Mater*, 2022, **32**, 2111740.

[4] H. Zhou, *et al*., Self-hydrogen Supplied Catalytic Fractionation of Raw Biomass into Lignin-derived Phenolic Monomers and Cellulose-rich Pulps, *JACS Au*, 2023, **3,** 1911-1917.

[5] Z. Dou, *et al*., Photocatalytic Upgrading of Lignin Oil to Diesel Precursors and Hydrogen, *Angew Chem Int Ed*, 2021, **60,** 16399-16403.

[6] H. Jiang, *et al*., Photocatalytic lignin oils and CO2 upgradation to diesel precursors and syngas over engineered CdSe quantum dots, *Cheml Eng J*, 2023, **471**, 144452.

[7] X. Wu, *et al*., Zinc-indium-sulfide favors efficient C−H bond activation by concerted proton coupledelectrontransfer, *Nat Commun*, 2024, **15**, 4967.